Self-Assembled Diamond Nanocrystals

B. Golding

Department of Physics & Astronomy

Michigan State University

E. Lansing, MI 48824 USA

Abstract

The initial stages in the growth of diamond from the vapor phase can lead to the appearance of dense, ordered arrays of diamond nanocrystallites. When diamond is condensed from a methane-hydrogen plasma onto (001) epitaxial iridium, orientationally-ordered (001) diamond nanocrystallites appear at a density 10^{12} cm^{-2}. They occur on the Ir surface after a rapid cooling brought about by abrupt termination of the plasma. The crystallite sizes are highly monodisperse, typically with lateral size 7 nm and mean interparticle spacing 14 nm. The emergent diamond crystals form a weakly ordered triangular lattice with correlation lengths of several lattice parameters. Possible explanations for the pattern formation include: depletion interactions, substrate-induced strain, or a spinodal mechanism. Because the crystallite density is so high, subsequent evolution leads to rapid coalescence within a few minutes, resulting in a smooth, continuous film that covers the substrate. When the growth step is extended in time, thick single crystal plates can be produced. These observations are useful for understanding diamond nucleation and growth as well as for developing reliable heteroepitaxial growth processes.

1. Introduction

It has been appreciated for several years that electronic devices based on diamond's large 5.5 eV bandgap would have many advantages over conventional small bandgap semiconductors. Steady progress in achieving semiconductor-grade material has occurred over the past few years. Most development efforts have focused on growth of diamond on diamond substrates, or *homoepitaxial growth*. Extremely good homoepitaxial diamond has been recently produced, with high electronic mobilities[1]. The major drawback to large-scale homoepitaxial growth arises from the need for large natural or synthetic diamond substrates.

Since an efficient process for producing large substrates is needed, research that focuses on *heteroepitaxial growth* may lead to an alternative technology. Previously, diamond grown on silicon has yielded highly-oriented crystallites[2-4] with thick films and plates prepared on large substrates that are suitable for infrared or microwave windows, lenses, and heat spreaders[5]. But with a mosaic spread greater than 1 angular degree, this material is not suitable as substrates for homoepitaxy. Furthermore, grain boundaries limit carrier mobility by introducing carrier trap states making highly-oriented diamond unsuitable for high performance electronic applications.

Heteroepitaxial growth depends on achieving uniform and high diamond nucleation densities across a substrate. The bias-enhanced nucleation process[6], in which a negative voltage applied to the substrate extracts low-energy positive ions from the plasma, is a key step for inducing the formation of diamond nuclei. There is little consensus on the underlying mechanism that induces nucleation. It is necessary for all nuclei to adopt the underlying orientation of the substrate; rapid coalescence of the diamond crystallites should occur early in the growth stage. Since lattice mismatch is inevitable in heteroepitaxy, strain plays an important role. With the large lattice mismatch between diamond and silicon substrates, most diamond nuclei do not adopt an epitaxial relationship, so highly-oriented films are obtained by choosing growth conditions that amplify a minority fraction of epitaxial crystallites.

A significant advance occurred when it was found that films of Ir, grown as a buffer layer on MgO, could serve as a substrate for the nucleation and growth of CVD diamond[7-9]. Ir is face-centered cubic, with a lattice parameter 7% larger than diamond, with good long-term chemical and physical stability, enabling it to withstand the high-temperature hydrogen plasma used in CVD diamond growth. The use of $SrTiO_3$ as a substitute for MgO has led to a reduction of the mosaic spread of the epitaxial Ir and the resultant heteroepitaxial diamond[10, 11]. More recently, it has been shown that a-plane sapphire can be used as a substrate for (001) Ir films, raising the possibility of large area (001) heteroepitaxial diamond films[12].

We summarize here the results of a series of experimental investigations of CVD diamond grown on epitaxial (001)Ir. The studies suggest possibilities for understanding and controlling large-area diamond heteroepitaxy at a level previously unrealized. The studies show that diamond nuclei can be formed at

high densities, all epitaxially aligned with the underlying substrate. The nanocrystallites that develop at an early growth stage, typically 7 to 8 nm in lateral extent, do not appear at random on the Ir surface but show spatial correlations that persist for large distances[13]. The patterns that form show similarities to self-organized structures that emerge in two-dimensional solidification[14], dewetting[15], and spinodal decomposition[16]. In view of the complexity of the CVD environment, the underlying mechanism or mechanisms have yet to be fully understood.

As a practical consequence of the dense early epitaxy, the crystallites coalesce to form a continuous single crystal diamond film within a few minutes of growth. Thick plates of diamond have been produced by extended growth runs, yielding materials that exhibit good transparency in visible light, and cleavage properties that mimic natural diamond. With judicious choice of substrate and biasing conditions it may not be long before wafer-scale single crystal diamond substrates are fabricated[12].

2. Experimental methods

Experiments were carried out on 5x5x0.5 mm^3 or 10x10x0.5 mm^3 substrates obtained from commercial sources. Descriptions of the substrate preparation have been given previously[13]. Ir growth on (001) $SrTiO_3$ and on $(11\bar{2}0)$ α-Al_2O_3, (a-plane sapphire) with a variety of vicinal surfaces was explored. Iridium was deposited at 850-950 ºC by electron-beam evaporation in a UHV system. With sapphire, the resulting Ir films were epitaxial with orientation Ir(001)|| Al_2O_3 $(11\bar{2}0)$ and Ir$[110]$|| Al_2O_3 $[1\bar{1}00]$[17]. X-ray rocking curves showed linewidths approaching 0.2 deg for 150 nm Ir films on both substrate systems.

Following Ir evaporation, the samples were cooled and transferred to a CVD chamber. The CVD system (2.45 GHz, 6 kW max, base pressure 10^{-8} Torr) and typical procedures have been previously described[13]. The process was initiated by a pure hydrogen plasma, followed by the addition of a 2% methane/hydrogen mixture. With the system at steady-state (18 Torr pressure), a negative bias was applied to the substrate. The temperature during bias was about 700 ºC, as measured by an optical pyrometer focused on the Ir surface. The bias voltage, in the range –140 to –200 V, was abruptly terminated after a predetermined time. This procedure subjected the sample to a rapid temperature quench. We now consider how the chemical and topographical features of the substrate evolve as a function of biasing duration.

3. Results

Examination of the Ir substrate by SEM revealed patterns characterized by strong secondary electron contrast which are interpreted as arising from sp^3 carbon. Since at this stage it is not necessarily diamond, we refer to it as a "condensate". For a bias period of 60 min, the areal coverage of the substrate by the bright condensate is approximately 82 %. Fig. 1 shows images of the quenched surface at successively greater magnification. On a scale of several μm, Fig. 1a, the substrate appears to be uniformly covered with condensate.

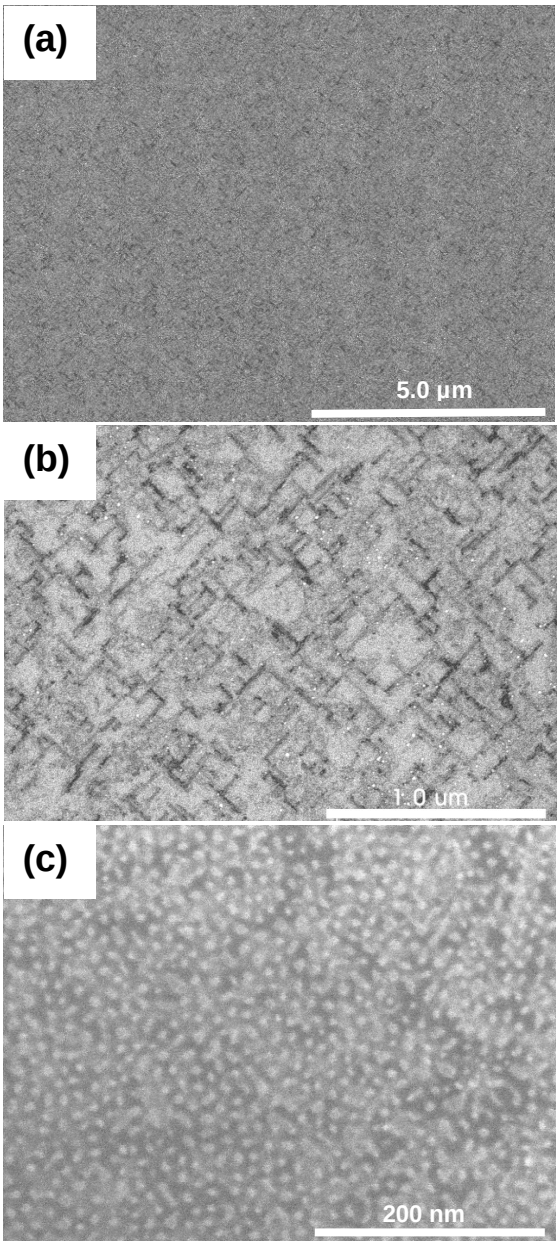

Fig. 1. Scanning electron microscope images of the (001) Ir surface after 60 min of biasing. The dark regions are Ir. Successively higher magnification of the same sample region is given in (a), (b), and (c). In (a), approximately 84% of the surface is covered with condensate; (b) shows the low-density regions with <110> alignment; (c) shows the diamond nano-crystallites[24].

With greater resolution, Fig. 1b, it can be seen that dark regions, representative of low condensate density, are present. They lie in bands parallel to the [110] directions. At the highest magnification in Fig. 1c, a completely new feature emerges. Here, the condensate has formed into clusters with diameters near 7 nm whose separation is approximately twice their diameter. There is a tendency for the clusters to order into a close-packed lattice.[13]

The SEM image in Fig. 1c also suggests that the clusters are embedded in a continuous matrix. The matrix is not uniform and we interpret the regions of low contrast to indicate a thinner condensate, as seen especially in the right side of the image. In these regions, the strong short range order of the clusters is disrupted. In comparison with the images at lower magnification, we see that these depleted regions are the dark, predominantly [110] bands that dominate Fig. 1b. They are essentially remnants of the ridges that were etched in the early stages of the biasing process. Although clusters still form in these regions, they are less likely to be uniform in size, less uniformly ordered, and show some coalescence.

At a later stage of growth, the crystallites coalesce to form a continuous thin film. We studied coalescence by interrupting growth at intervals from a few seconds to several minutes following the end of biasing. The high degree of coalescence that occurs after only a few minutes of growth is shown in Fig. 2 and has been previously documented.[13] After 60 minutes of growth, the films are continuous

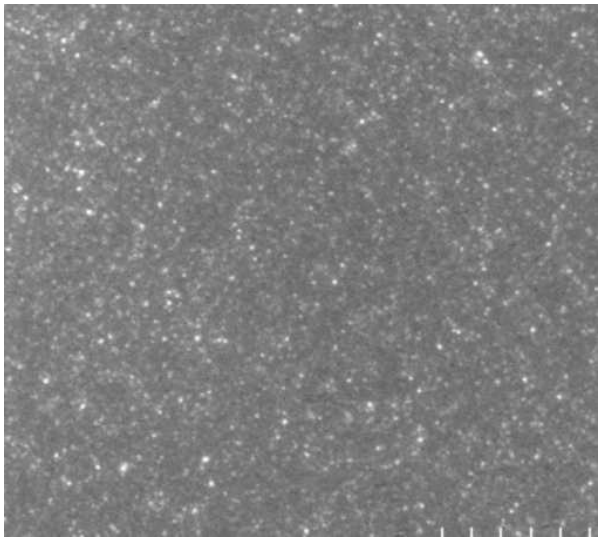

Fig. 2. Scanning electron microscope images of the (001) surface of heteroepitaxial diamond on (001)Ir/(a-plane sapphire) after 60 minutes of CVD growth. The bright spots correspond to enhanced electron emission from small topographic features. Tick spacing: 500 nm.

across the entire substrate and are quite smooth. The results are consistent with the development of single crystal (001) diamond, with no evidence for misoriented or twinned regions. This implies that the clusters observed after the bias quenching are nanocrystals of diamond, all of which exhibit the same epitaxial relationship with the substrate. To confirm this hypothesis, a series of surface spectroscopy studies using X-ray photoelectron spectroscopy (XPS) and X-ray photoelectron diffraction (XPD) were initiated.[18] In particular, XPD is sensitive to the crystallinity and alignment of the ensemble of crystallites on the surface. By observing the anisotropy of the diffraction pattern it was concluded that the crystallites are oriented with respect to each other. The pattern was similar to that observed for diamond nucleating on diamond after the initial stages of homoepitaxial growth. The only difference was a slight decrease in the anisotropy, which was attributed to the presence of the uncrystallized carbon condensate that may cover some of the crystallites at this stage.

A surprising feature of the dots is their remarkable uniformity. Isolated dots have a size distribution that peaks between 7 and 8 nm. In some instances, larger dots are found, but they usually are the result of the coalescence of two or more dots. In addition, the spatial arrangement of the dots is not random, as inspection of Fig. 1c shows that the spacing between dots is quite uniform. The arrangement is almost close-packed, with a mean dot-dot spacing of 14 to15 nm, roughly twice their average diameter. A measure of their correlations can be obtained by computing the radial density function, g(r). This is the probability of finding a dot in a band between r and r+δr from a dot at the origin. It is numerically calculated for a surface area containing approximately 300 dots and is shown in Fig. 3. The largest peak occurs at r_{nn} = 14 nm, which represents the mean nearest-neighbor (nn) distance. Additional peaks occur at larger values of r, indicating significant correlations out to 4^{th} and possibly 5^{th} nearest neighbors. If one assumes that the dots can be described as a weakly disordered 2-d triangular net with edge length r_{nn}, then positions of n^{th} neighbors are shown by the dashed lines in Fig. 3. The broad peaks in g(r) near 27 and 40 nm are consistent with this symmetry.[18]

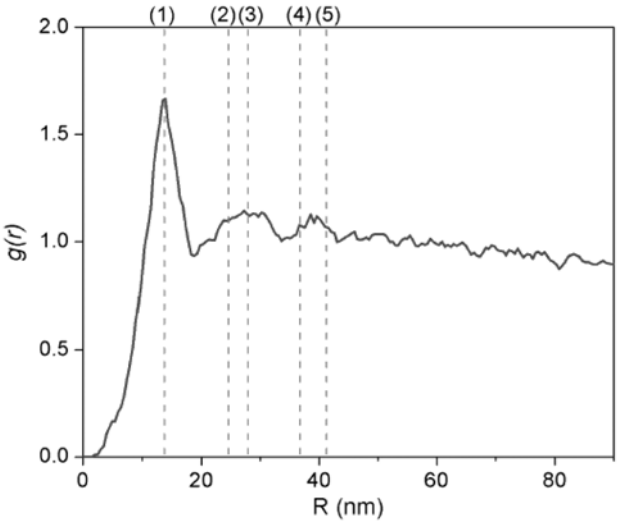

Fig. 3. Radial density function for diamond dots. The function was computed by analyzing SEM images similar to that shown in Fig. 1. Approximately 300 dots were used in the calculation (Ref. 18).

The length scale associated with the dot lattice is much larger than the underlying Ir lattice. The symmetry is also inconsistent with the (001) surface of an unreconstructed Ir layer. Although reconstructions of the Ir surface under UHV conditions have been seen, their periodicity is much smaller than the scale of the dot lattice. Ridges that propagate along the [110] directions of the (001)Ir surface have been observed after exposure to the hydrocarbon plasma. These appear during etching of the Ir surface in the hydrogen plasma and may contribute to the disorder of the dot array since they occur more or less randomly on the surface. It is reasonable to conclude that the dots organize spontaneously on the surface in a short interval following the termination of the bias. We hypothesize that they result from the nucleation and growth of diamond nanocrystals from a precursor matrix that is deposited on the surface of the Ir during the bias process. Correlations develop during the growth period, through depletion interactions and strain, and these correlations lead to a close-packed arrangement. Variations in surface topography, due to etching of the Ir surface, interrupt the self-organization process, leading to the finite correlation length.

Surface topography was studied with atomic force microscopy (AFM). Figure 4 (left) shows a 500 nm x 500 nm scan of an Ir surface, biased for 60 min, and then rapidly cooled. Two motifs are visible: the small peaks, identified as diamond dots, and long ridges. The ridges rise 6 to 7 nm above the local minima in their vicinity. To assess the topography of the dots, we examined the small region inside the box in the upper part of the scan. The right side of Fig. 4 shows a plan view of this region using phase contrast imaging. Interdot distances, measured from a central dot, are between 13 and 20 nm, consistent with the data in Figs. 1 and 3, whereas their maximum height differences vary from 0.1 to 0.6 nm in this region. AFM does not allow us to find the height of the dots above the Ir film since it provides no chemical information. However, the height variation within the cluster of dots is no more than 1 to 2 nm, much less than the diameter of the dots. There may be several explanations for this result. For example, it is possible that the dots are not spherical but are flattened in the direction normal to the surface. Alternatively, nearly spherical dots may be embedded in a smooth matrix that shows weak electron contrast in the SEM. SEM micrographs usually

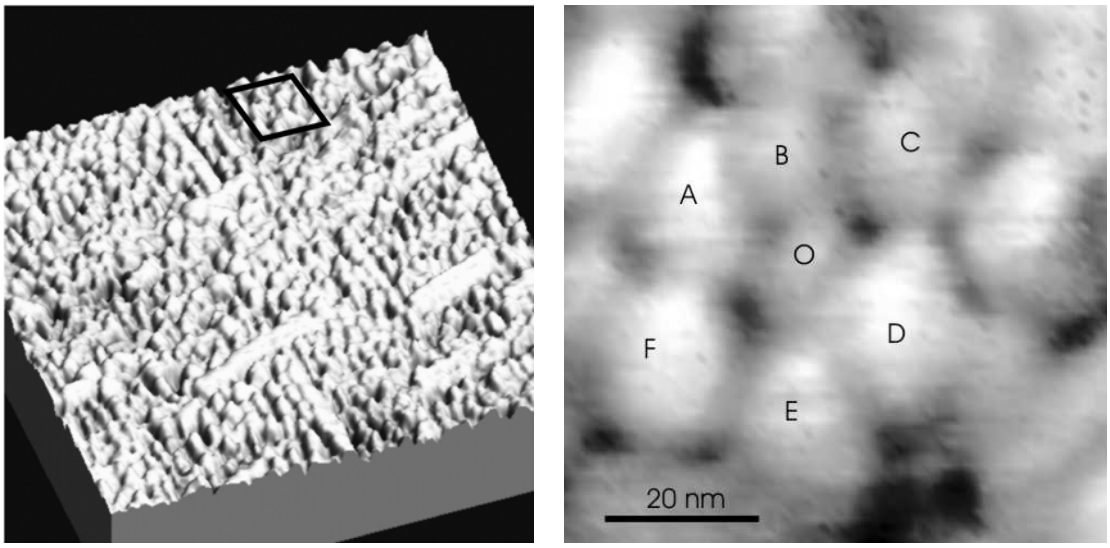

Fig. 4. (Left) AFM image of a 500 nm x 500 nm region of the surface of bias-treated Ir(001) surface. Note the dense array of small islands (dots) as well as long ridges. The ridges originate during etching of the Ir by the hydrogen plasma. (Right) Expansion of the region inside the small box at the top. Note the six dots (A-F) surrounding a central dot (O) (see Ref. 18).

show smooth contrast variation on a scale greater than the interdot distance which could arise from thickness variation of the matrix.

To explore the properties of thicker diamond films, we carried out growth for longer periods, 3 to 12 hr. Growth proceeded for 90 minutes with a CH_4/H_2 ratio of 1%. Then, the total gas pressure was raised to 28 Torr with the CH_4/H_2 ratio left the same or decreased to 0.75%. For this growth period, stress accumulation between diamond and oxide substrate usually leads to delamination of the film on cooling. The Ir film adheres to the diamond; the $Ir/SrTiO_3$ interface is ruptured. Fig. 5 shows a region of such a film that spontaneously cleaved along principal crystallographic axes. The film is clearly a single crystal with a smooth and flat (001) surface.

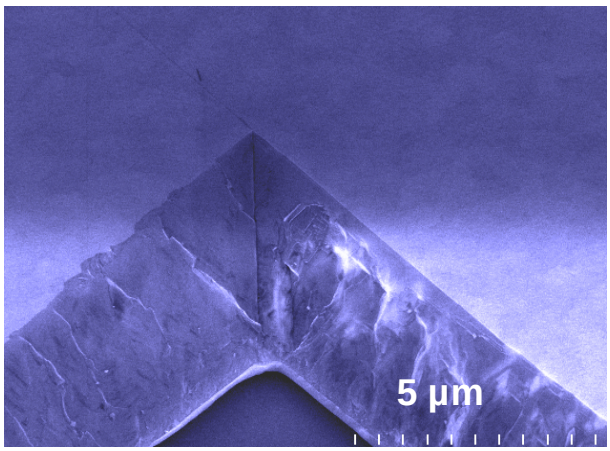

Fig. 5. SEM image of a thin diamond film grown for 4.5 hr. The film delaminated spontaneously from the substrate on cooling creating the picture frame structure. Note the smooth (001) growth surface, the [110] fracture directions and the [111] fracture surfaces.

Diamond (001) slabs with thickness from 25 to 38 µm have also been grown. The thickest crystals are transparent in visible

Fig. 6. Single crystal of (001) diamond grown by CVD on a Ir/$SrTiO_3$ substrate. The diameter is 3.5 mm; thickness is 35 μm. Note the absence of optical aberration and misoriented regions[24].

light when the Ir epilayer is etched away. Polarized Raman spectroscopy shows that the crystals obey the selection rules expected for light wavevectors parallel to [001] and [110] directions in backscattering geometry. The spectra are shifted with respect to the natural diamond stretching mode frequency indicating the presence of internal stress. The spectra are not dependent on the depth or lateral position of the excitation focus, indicating that internal stress is homogeneous throughout the crystal volume. Fig. 6 shows an optical micrograph of a 35 μm diamond crystal grown by heteroepitaxy. The edge is parallel to the <110> direction with a (111) cleavage surface. At this thickness the diamond will occasionally delaminate from the substrate and residual stress may lead to fracture of the substrate but not usually the diamond itself. The crystal has good optical quality a result of low macroscopic defect density and the smoothness of the surfaces.

4. Discussion

During the bias process, the system is in intimate contact with a hot hydrocarbon plasma. On terminating the bias, a thermal quench takes place in a fraction of second and leaves the condensate far from equilibrium. The system evolves to a locally stable state which can then be probed by characterization tools. With this static approach, one cannot unambiguously determine the state of the system before the quench. Therefore, inferences must be made based on plausible scenarios that could lead to the post-quench patterns revealed in Fig. 1. With relatively few assumptions, it is possible to make some general observations regarding the initial appearance of diamond.

- The biasing process leads to the deposition of a thin layer of carbon at the surface of the iridium. The thickness, as well as coverage, of the layer increases with bias duration.
- During biasing, the hydrogen plasma etches the Ir surface with a degree of roughening dependent on the reactor conditions.
- Some inadvertent nucleation of diamond may occur at topographic features, such as ridges or step edges, on the Ir surface.
- When the carbon deposit becomes sufficiently thick, self-organized diamond nanocrystals appear after a bias quench (Fig. 1c). The arrays have only weak correlations with substrate topography or crystallography.

- The ordered array of nanocrystallites appears synchronously with the thermal quench that accompanies the termination of the bias process.
- The topographic relief of the substrate creates disorder that interferes with self-assembly and foreshortens the intercluster radial correlations.

A scenario that is consistent with these observations is the following sequence of events In the presence of the hot plasma discharge during biasing, the thin carbon condensate is highly excited. It acquires a relatively high atomic mobility. When the bias is removed, the condensate cools rapidly and finds itself momentarily far from equilibrium. Diamond nanocrystallites emerge out of the supercooled condensate at the Ir interface. The simultaneous occurrence of the diamond crystals suggests a homogeneous process. Since diamond is a denser phase than its precursor, some depletion of the condensate occurs and the crystallites grow. They are limited in lateral extent by strain and by the rate at which dislocations evolve. Eventually, steady state growth from the vapor phase becomes the dominant process. When the crystallite sizes reach the intercluster distance, they readily coalesce to form a continuous diamond film.

Two questions need to be addressed: (a) what is the nature of the process that creates the diamond nanocrystals, and (b) what is the nature of the precursor phase out of which diamond forms? The conventional picture of a first-order phase transition is based on classical nucleation; a supercritical density fluctuation occurs which forms a stable diamond cluster[19]. A typical critical nucleus is smaller than the nanocrystals observed in Fig. 1c (mean diameter 7 nm) so that some growth beyond the critical size has occurred before diffusion is arrested by the quench. This picture of random nucleation must be reconciled with the highly monodisperse, well-ordered array of crystals with density 5×10^{11} cm^{-2} seen in Fig. 1c. For consistency with a random process, the nuclei must initially form at a density one to two orders of magnitude greater than that of the clusters. Self-organization can then occur only if some nuclei continue to grow at the expense of others. Screening can lead to dipolar-like interactions and, if the mobility is sufficiently high, ordering can appear[20,21]. This argument does not explain the uniform size distribution observed, however. Since nucleation is thermally activated, there is a Poissonian distribution of waiting times which would not lead to a narrow size distribution. However, it is possible that nucleation rates are sufficiently slow that a distribution is not readily apparent.

An alternative explanation for the periodicity and monodispersivity is based on a global, as opposed to a local, instability. The condensate decomposes by a spinodal mechanism, which does not involve an activation barrier[22]. In this picture, density fluctuations with a restricted spectrum of wavevectors become unstable following a rapid quench. Spectral narrowing occurs rapidly so that a dominant spatial frequency emerges that results in a periodic-looking structure. Examples of systems in which large-scale instabilities have been identified are often isotropic, such as near-critical fluids, glasses, and polymers. In anisotropic systems, strain must be taken into account[16]. Electric-field induced instabilities have also been suggested[23] that could potentially apply to the present situation. In the advanced stages of decomposition the spinodal-growth and nucleation-

growth mechanisms are difficult to distinguish[19]. The nature of the non-equilibrium precursor phase of carbon remains unclear, although from energetic considerations it cannot differ significantly from sp^3 bonded diamond.

5. Conclusions

The patterns that emerge in heteroepitaxial growth of diamond are leading to alternate ways of identifying the underlying physical mechanisms responsible for the process. Perhaps the most interesting is the idea that order spontaneously appears after biasing is terminated, manifested by the self-organization of diamond nanocrystallites. The six-fold, close-packed lattice has symmetry incompatible with the cubic Ir substrate surface, and it occurs on the scale of 100 times the Ir interatomic distance. It is only weakly pinned by the substrate, most likely by plasma-induced roughening of the Ir surface.

We have shown that significant improvements in the heteroepitaxial growth of diamond using a (001) Ir buffer layer are possible. As a consequence of the dense nanocrystallite density, coalescence takes place at a very early stage of growth, leading to highly oriented films with low defect densities. Growth of thick single crystal films has been described here (Fig. 6). Long growth times place demands on system stability and cleanliness. Nevertheless, the overall structural, optical, and electrical properties of these laboratory grown diamond single crystals is improving steadily. Coupled with better quality substrates, such as a-plane sapphire, we expect that it will not be long before wafer-scale electronic grade diamond substrates become available.[24]

Acknowledgements

This work was done in collaboration with Connie Bednarski-Meinke, Zhong-ning Dai, and An-Ping Li. We thank B. Bi for assistance with electron microscopy and AFM. We acknowledge use of the Keck Microfabrication Facility and support from the National Science Foundation under MRSEC program grant DMR-9809688.

References

1. J. Isberg, J. Hammersberg, E. Johansson, T. Wikstrom, D. J. Twitchen, A. J. Whitehead, S. E. Coe and G. A. Scarsbrook, Science 297 (2002) 1670.
2. S. Wolter, B. Stoner, J. G. P. Ellis, D. Buhaenko, C. Jenkins and P. Southworth, Appl. Phys. Lett. 62 (1993) 1215.
3. X. Jiang, R. Six, C. P. Klages, R. Zachai, M. Hartweg and H. J. Fusser, Diamond and Relat. Mater. 2 (1993) 407.
4. C. Wild, N. Herres, R. Locher, W. Mueller-Sebert and P. Koidl, In Advances in New Diamond Science and Technology, ed. K. Kobashi & M. Yoshikawa, Tokyo, 1994, pp. 149.
5. A. Flöter, H. Guttler, G. Schulz, D. Steinbach, C. Lutz-Elsner, R. Zachai, A. Bergmaier and G. Dollinger, Diamond and Relat. Mater. 7 (1998) 283.
6. S. Yugo, T. Kanai, T. Kimura and T. Muto, Appl. Phys. Lett. 58 (1991) 1036.
7. K. Ohtsuka, K. Suzuki, A. Sawabe and T. Inuzuka, Jpn. J. Appl. Phys. Pt. 2 35 (1996) L1072.
8. K. Ohtsuka, H. Fukuda, K. Suzuki and A. Sawabe, Jpn. J. Appl. Phys. Pt. 2 36 (1997) L1214.
9. T. Tsubota, M. Ohta, K. Kusakabe, S. Morooka, M. Watanabe and H. Maeda, Diamond and Relat. Mater. 9 (2000) 1380.
10. M. Schreck, H. Roll and B. Stritzker, Appl. Phys. Lett. 74 (1999) 650.
11. M. Schreck, F. Hörmann, H. Roll, J. K. N. Lindner and B. Stritzker, Appl. Phys. Lett. 78 (2001) 192.
12. Z. Dai, C. Bednarski-Meinke, R. Loloee and B. Golding, Appl. Phys. Lett. 82 (2003) 3847.
13. C. Bednarski, Z. Dai, A.-P. Li and B. Golding, Diamond and Relat. Mater. 12 (2003) 241.
14. R. Plass, J. A. Last, N. C. Bartelt and G. L. Kellogg, Nature 412 (2001) 875.
15. S. Herminghaus, K. Jacobs, K. Mecke, J. Bischof, A. Fery, M. Ibn-Elhaj and S. Schlagowski, Science 282 (1998) 916.
16. A. Onuki and A. Furukawa, Phys. Rev. Lett. 86 (2001) 452.
17. R. Vargas, T. Goto, W. Zhang and T. Hirai, Appl. Phys. Lett. 65 (1994) 1094.
18. S. Kono, M. Shiraishi, N.I. Plusnin, T. Goto, Y. Ikejima, T. Abukawa, M. Shimomura, Z. Dai, C. Bednarski-Meinke and B. Golding, New Diamond and Frontier Carbon Technology, (to be published, 2005).

19. J. S. Langer, In Solids Far from Equilibrium, ed. C. Godreche. Alea Saclay, Cambridge, 1991, pp. 297.

20. O. L. Alerhand, D. Vanderbilt, R. D. Meade and J. D. Joannopoulos, Phys. Rev. Lett. 61 (1988) 1973.

21. K. Ng and D. Vanderbilt, Phys. Rev. B (1995) 2177.

22. J. W. Cahn and J. E. Hilliard, J. Chem. Phys. 28 (1958) 258.

23. S. Herminghaus, Phys. Rev. Lett. 83 (1999) 2359.

24. B. Golding, C. Bednarski-Meinke, and Z. Dai, Diamond and Relat. Mater. 13 (2004) 545.